Methanol Selective Oxidation to Dimethoxymethane and Methyl Formate over Monolayer V_2O_5/TiO_2 Catalyst

V.V. Kaichev[a,b,*], G.Ya. Popova[a], Yu.A. Chesalov[a], A.A. Saraev[a], D.Y. Zemlyanov[c], S.A. Beloshapkin[d], A. Knop-Gericke[e], R. Schlögl[e], T.V. Andrushkevich[a], V.I. Bukhtiyarov[a,b]

[a] *Boreskov Institute of Catalysis of SB RAS, Lavrentieva ave. 5, 630090 Novosibirsk, Russia*

[b] *Novosibirsk State University, Pirogova st. 2, 630090 Novosibirsk, Russia*

[c] *Birck Nanotechnology Center, Purdue University, 1205 West State Street, West Lafayette, IN 47907-2100, USA*

[d] *Materials and Surface Science Institute, University of Limerick, Limerick, Ireland*

[e] *Fritz-Haber-Institute of MPG, Faradayweg 4-6, D-14195 Berlin, Germany*

[*] Corresponding author. Fax: +7 383 330 80 56.
E-mail address: vvk@catalysis.ru (V.V. Kaichev).

A B S T R A C T

The methanol oxidation over highly dispersed vanadium oxide supported on TiO_2 (anatase) has been investigated by *in situ* Fourier transform infrared spectroscopy (FTIR), near ambient pressure X-ray photoelectron spectroscopy (NAP XPS), X-ray absorption near edge structure (XANES), and temperature-programmed reaction spectroscopy. The data were complimented with kinetics measurements in a flow reactor. It was found that at low temperatures dimethoxymethane competes with methyl formate, whereas the production of formaldehyde is greatly inhibited. FTIR shows the presence of non-dissociatively adsorbed molecules of methanol, as well as adsorbed methoxy, dioximethylene, and formate species under reaction conditions. According to the NAP XPS and XANES data, the reaction involves the reversible reduction of V^{5+} cations, pointing that the vanadia lattice oxygen participates in the methanol oxidation through the classical Mars-van Krevelen mechanism. The detailed mechanism of the methanol oxidation on vanadia catalysts is discussed.

Keywords:

Methanol oxidation

Vanadium pentoxide

Monolayer catalyst

Near ambient pressure X-ray photoelectron spectroscopy

1. Introduction

The methanol oxidation over V_2O_5/TiO_2 catalysts is of both fundamental and practical interests. On the one hand, this is the excellent example of a relatively simple reaction of selective oxidation, which can produce a wide range of various compounds such as formaldehyde (F), dimethyl ether (DE), methyl formate (MF), dimethoxymethane (DMM), and formic acid (FA) with the selectivities that depend on a catalyst, reaction temperature, conversion, and partial pressures of reactants [1-4]. For instance, unsupported and silica-supported crystallites of vanadium pentoxide show high selectivity towards formaldehyde with the yield of 96-98 % in the temperature range of 300-400 °C [5-8]. In contrast, monolayer V_2O_5/TiO_2 catalysts demonstrate high activity and selectivity in the methanol oxidation to methyl formate and to dimethoxymethane at low temperatures (100-200 °C), whereas the formation of formaldehyde is greatly suppressed [9-22]. On the other hand, all products mentioned above are of practical significance. For instance, production of formaldehyde via the methanol oxidation is one of the most important industrial catalytic processes. Besides, vanadia-based catalysts can be used for production of methyl formate and dimethoxymethane (methylal), both of which are important and versatile chemicals. Methyl formate is mainly used to manufacture formamide, dimethylformamide, and formic acid [23,24]. Dimethoxymethane is primarily used as a solvent and in the production of perfumes, resins, adhesives, paint strippers, and protective coatings. Dimethoxymethane is an environment friendly material with extremely low toxicity and it may be also used as a H_2 storage material for compact hydrogen generators [25,26].

Nowadays, the industrial production of methyl formate takes place through the carbonylation of methanol with carbon monoxide over sodium methoxide catalysts in the liquid phase [23]. Due to high catalyst sensitivity to water, dry CO must be used in this process. Dimethoxymethane is currently produced via a two-stage process involving (1) the methanol oxidation to formaldehyde on silver or iron-molybdate catalysts followed by (2) condensation reactions in a methanol-formaldehyde mixture using sulfuric acid or solid acid catalysts. Therefore,

the development of efficient catalysts for one-stage synthesis of both MF and DMM through methanol oxidation in the gas phase has a great practical interest, and the V_2O_5/TiO_2 catalyst is one of the perspective candidates.

The V_2O_5/TiO_2 system has been actively studied over the last thirty years. It was found that vanadia on a titania surface forms different types of structures depending on the vanadia content and the preparation technique [27-34]. At vanadia content below 10 % of monolayer (ML), only a monomeric isolated structure exists, which has a tetrahedral coordination (VO_4) in dehydrated conditions [29,33]. When vanadia concentration is above approximately 20 % of ML, polymeric structures (chains and ribbons of VO_x units) with an octahedral coordination (VO_6) appear [33]. These structures may change under reaction conditions through reduction/oxidation or hydration/dehydration; however, these changes are confined on the surface, and migration of cations to or from the sub-surface region does not occur at ambient temperature [29]. The incorporation of V^{4+} cations into the crystal lattice of TiO_2 has been observed at temperatures above 600 °C during anatase-to-rutile transformation in the V_2O_5/TiO_2 catalysts [35]. Monolayer surface coverage of polymerized vanadia species on different oxide supports was measured by Raman spectroscopy and was found to be approximately 7-8 V-atom/nm^2 for TiO_2 [31]. At the vanadium content above the ideal monolayer, V_2O_5 crystallites are favorable. On the other hand, the V_2O_5 crystallites are relatively inactive and non-selective comparing to the surface vanadia species in the wide range of catalytic reactions [36,37]. The unique properties of the surface vanadia species are related to the strong vanadia-support interaction.

This work reports the catalytic properties of highly dispersed vanadium oxide supported on TiO_2 (anatase) in the selective methanol oxidation in the gas phase. Selectivity and reaction rates were found to be dependent on the reaction temperature. Dimethoxymethane is the main reaction product at the temperatures below 120 °C with selectivity up to 95 %. A sharp decrease in the selectivity to DMM and an increase in the selectivity to MF were observed above 120 °C. At 140-150 °C methyl formate prevails among the products and the selectivity reaches 90 %. To provide

further insight into the reaction mechanism, near ambient pressure X-ray photoelectron spectroscopy (NAP XPS), X-ray absorption near edge structure (XANES), Fourier transform infrared spectroscopy (FTIR), X-ray diffraction (XRD), and temperature-programmed reaction (TPR) were used. The main conclusion is that the lattice oxygen is involved in the methanol oxidation via the classical Mars-van Krevelen mechanism.

2. Experimental

2.1. Catalyst preparation

A two-step procedure was used for preparation of the monolayer V_2O_5/TiO_2 catalyst. The first step was the incipient-wetness impregnation of the TiO_2 support (anatase, 350 m^2/g) with an aqueous solution of vanadyl oxalate followed by drying at 110 °C for 12 h and final calcination in air flow at 400 °C for 4 h. This catalyst was referred to as "fresh". The fresh catalyst (20 wt% V_2O_5 and 80 wt% TiO_2) was then treated in 10 % aqueous solution of nitric acid at room temperature. After the washing the catalyst (12.5 wt% V_2O_5 and 87.5 wt% TiO_2) was calcined in air flow at 400 °C for 4 h. This catalyst was referred to as "washed". As it is shown below morphology of this catalyst corresponds to so-called structure of monolayer catalyst.

2.2. Catalytic tests

The steady-state activity of the catalysts was tested at atmospheric pressure in a differential reactor of a flow-circulating setup [38]. The reactor was made from Pyrex glass tube of 12 mm inner diameter with length of 50 mm. For temperature control a coaxial thermocouple pocket of 4 mm outer diameter was fitted in the catalyst bed. The reactor was placed inside of an oven. The temperature was controlled with accuracy of ±0.5 °C. The catalyst fraction from 0.25 to 0.5 mm was used in the experiments. The feed composition consisted of methanol, oxygen, and nitrogen in the molar ratio of 1:1:12. The concentrations of reactants and products were determined by an on-line gas chromatograph (GC) equipped with thermal conductivity detector and flame ionization detector. Methanol, dimethoxymethane, methyl formate, formaldehyde, formic acid, water, and CO_2

were analyzed using a Porapak T column, whereas CO, oxygen, and nitrogen were analyzed using a NaA molecular sieve column. All gas lines from the reactor to the sampling valve were kept at 120 °C to prevent condensation of the reactants and products. The selectivity, S_i, was calculated as the molar concentration of carbon appurtenant, c_i, of product *i* divided by the sum of the concentrations of all products, $S_i = c_i/\Sigma c_j \times 100$ %. The carbon balance was at least 97±2 % for all GC measurements.

2.3. Catalyst characterization

Catalysts were characterized by X- ray diffraction, N_2 adsorption, elemental analysis, and FTIR spectroscopy. Powder XRD measurements were performed using a D500 diffractometer (Siemens) with the monochromatic Cu K_α radiation. 2θ scan covers the range of 5-70°. The specific surface area was calculated by the BET method from nitrogen adsorption isotherms measured at liquid nitrogen temperature on an automatic ASAP 2400 Sorptometer (Micromeritics). Elemental analysis was performed using an ICP atomic emission spectrometer (ICP, Baird). IR spectra were recorded using a FTIR spectrometer MB-102 (BOMEM). The IR samples were tablets of the catalysts or the TiO_2 powder pressed together with CsI (2 mg of the sample and 500 mg of CsI).

2.4. In situ characterization

The chemical states of catalysts were examined *in situ* by NAP XPS and XANES techniques. The experiments were performed at the synchrotron radiation facility BESSY II, Berlin, using the ISISS (Innovative Station for *In Situ* Spectroscopy) beamline. The experimental system was described in detail elsewhere [39]. The key feature of this system is *in situ* measurements of photoemission spectra under mbar pressures. High brilliance synchrotron radiation together with a short flying path of the photoelectrons through the high-pressure zone in the gas cell allows us to obtain high-quality spectra at pressure up to 10 mbar in flow regime. Powder samples were pressed into a thin self-supporting tablet and then mounted at a sapphire holder between SiC and stainless steel plates. The heating was done from the rear with a near-infrared semiconductor laser (λ = 808 nm). The sample temperature was measured using a chromel-alumel thermocouple pressed directly

against the sample rear. The methanol and oxygen flows into the gas cell were regulated separately with calibrated mass-flow controllers. The flow rate of the reaction mixture was approximately 3 sccm. During the experiments, the total pressure of reaction mixtures in the gas cell was kept at a constant level of 0.25 mbar. The XANES spectra were collected in the total electron yield mode. The NAP XPS spectra were measured with the photon energy of 730 eV. All spectra were normalized to the ring current. The charge correction was done by setting the Ti $2p_{3/2}$ at 459.0 eV. The curve-fitting was performed using the CasaXPS software assuming a Lorentzian-Gaussian line-shape after a Shirley background subtraction.

For TPR, a sample was heated from 50 to 200 °C in a reaction mixture at a constant rate of 10 K/min. The gas-phase products were analyzed using an on-line quadruple mass-spectrometer (Prizma QMS-200, Balzers) connected through a leak valve directly to the gas cell.

In order to identify reaction intermediates involved in the methanol oxidation, FTIR spectra were also obtained *in situ* using the BOMEM MB-102 spectrometer. The spectrometer was operated in the transmission mode using a specially designed quartz cell-reactor with CaF_2 windows. The cell volume was 1.5 cm^3. The catalyst was pressed into thin self-supporting tablet (~15 mg/cm^2) and was placed into the cell-reactor. The FTIR experiments were performed at atmospheric pressure using a feed of 2 vol% CH_3OH in air with flow rate of 50 sccm. The spectra were recorded in the range of 4000-1100 cm^{-1} at a resolution of 4 cm^{-1} at different temperatures in the range of 50-180 °C. Prior exposing to a reaction mixture, the sample was treated in air flow at 300 °C for 60 min. Then the cell-reactor with the catalyst sample was cooled to a desired temperature, and air flow was replaced by the methanol/air mixture flow.

3. Results

3.1. Catalyst characterization

Fig. 1 shows the X-ray diffraction patterns of the fresh and washed V_2O_5/TiO_2 catalysts and the TiO_2 support. All peaks observed in the TiO_2 XRD pattern can be indexed to a pure tetragonal anatase phase (JCPDS File, No. 21-1272), while the XRD signatures of anatase and V_2O_5 are

observed from the fresh V_2O_5/TiO_2 catalyst. Vanadia coverage for this catalyst, which was estimated on the basis of the specific surface area and the vanadia content, is about 1.5 ML (Table 1). No XRD pattern of the vanadia crystalline phase is observed from the washed catalyst because nitric acid selectively dissolves V_2O_5 crystallites, whereas the highly dispersed vanadia species remain on the titania surface [34]. The amount of the insoluble vanadia is approximately a monolayer (Table 1). It means that in the washed catalyst, vanadium oxide is only in the highly dispersion state.

The presence of highly dispersed vanadia species in both the fresh and washed V_2O_5/TiO_2 catalysts was confirmed by FTIR. Fig. 2 shows the FTIR spectra of the fresh and washed catalysts, TiO_2 anatase, and bulk V_2O_5. In good agreement with the literature [40-42], the anatase phase of TiO_2 exhibits broad intensive absorption bands at 260-360 and 400-850 cm^{-1}. The spectrum of the fresh catalyst is a superposition of the anatase spectrum with weak, but well resolved, bands at 800-1030 cm^{-1}. After subtraction of the anatase spectrum, these features appear as a sharp band at 1015 cm^{-1} and broader bands at approximately 946 and 856 cm^{-1}. According to the literature data, the bulk V_2O_5 is characterized by the peaks at 1021, 828, 605, and 480 cm^{-1} [40,41,43]. The peaks at 1021 and 828 cm^{-1} were assigned to the V=O stretching and the deformation of V-O-V bridges, respectively. The broad band at approximately 600 cm^{-1} was assigned to the bending vibrations [43,44]. The peaks at 1015 and 856 cm^{-1} in the FTIR spectrum of the fresh catalyst (Fig. 2) confirm the presence of the V_2O_5 crystalline phase. However, the band at 946 cm^{-1} should be assigned to another species as it follows from comparison of FTIR spectra of the fresh and washed catalysts. Consistently with the XRD analysis, the intensities of the bands at 1015 and 856 cm^{-1} decrease substantially after the treatment in the aqueous solution of nitric acid, while the band at 946 cm^{-1} does not change (Fig. 2). Therefore, this band could be assigned to the V-O-Ti vibration of surface vanadate species. This assignment is consistent with the literature [40-42].

The conclusion is that the washed catalyst is mainly covered with approximately a monolayer of the highly dispersed vanadia species. The polymeric vanadia species dominate, while

the surface concentration of the isolated monomeric and dimeric vanadia species should be negligible. This fact was confirmed by Raman spectroscopy [45]. Typically, this catalyst is referred to as a monolayer catalyst [29].

3.2. Catalytic performance

The methanol oxidation by molecular oxygen was examined on the washed V_2O_5/TiO_2 catalysts between 70 and 150 °C. The molar methanol/oxygen ratio was kept equal to 1:1. Dimethoxymethane ($H_2C(OCH_3)_2$), methyl formate ($HCOOCH_3$), formaldehyde (HCHO), formic acid (HCOOH), carbon oxides (CO and CO_2), and water were detected as products. No dimethyl ether and other organic compounds were detected over the whole temperature range. Conversion and selectivity of each product at different temperatures, catalyst loading, and feed flow-rate are presented in Table 2.

The conversion of methanol increases with the temperature and with the catalyst loading, whereas it decreases at high feed flows (see, for example, at 120ºC highlighted with bold in Table 2). The methanol conversion is also affected by the methanol/oxygen ratio. For example, increasing the molar methanol/oxygen ratio from 0.5 to 2.7 at 175 °C decreases the methanol conversion from 100 to aproximatelly 30 % [9,11].

It should be also noted that pure TiO_2 (anatase) did not show any measurable methanol conversion up to 200 °C. This agrees with the literature data, which indicate that TiO_2 shows a high level of methanol conversion above 300 °C with CO and CO_2 as the main products [46].

Table 2 shows also the product distribution, which strongly depends on the reaction temperature. Between 70 and 100 °C dimethoxymethane is the main reaction product with selectivity of 80-95 %. Then the DMM selectivity decreases with the reaction temperature and the reaction shifts towards methyl formate. Between 140 and 150 °C methyl formate becomes the main reaction product. The formation of small amounts of formaldehyde, formic acid, CO, and CO_2 was also observed. The conversion of methanol also has an influence on selectivity (Table 2). Comparison of the data at 120^{o}C (highlighted with bold in Table 2) indicates that at the higher

methanol conversion, the selectivity towards DMM is lower, whereas the selectivity to MF is higher. For this reason, the methanol oxidation was examined at a constant methanol conversion.

Fig. 3 demonstrates the effect of the reaction temperature on the rate and the selectivity at 50 % methanol conversion. The rates of MF, F, FA, and CO_x increase with the temperature, while the DMM rate has a maximum at 130 °C. At low temperatures, DMM is the main reaction product. Above 120 °C, the DMM selectivity decreases and the MF selectivity increases. Methyl formate is the main reaction product between 140 and 150 °C. As shown by Busca et al. [9-11], the MF selectivity decreases above 170 °C and at 190-200 °C, carbon monoxide becomes the main reaction product.

3.3. In situ FTIR study

Fig. 4 shows the FTIR spectra acquired under the steady-state conditions during the methanol oxidation at different temperatures. The reaction mixture of 2 % CH_3OH in air was passed through the IR cell-reactor loaded with the washed V_2O_5/TiO_2 catalyst. The spectrum from the catalyst non-exposed to the reaction mixture and the spectrum from gas-phase methanol were subtracted from the raw IR spectra to identify the contribution from adsorbed surface species. One can see that at low temperatures up to 120 °C the methoxy species ($-OCH_3$) is the most abundant reaction intermediate. This conclusion was drawn from the observation of two intensive peaks at 2931 and 2825 cm^{-1}, which, according to the previous studies [9,13,47-53], correspond to the symmetric stretching $\nu_s(CH_3)$ mode and the Fermi resonance of $2\delta_s(CH_3)$ of the adsorbed methoxy species, respectively. The peaks at 2955 and 2847 cm^{-1} could be assigned to the same vibration modes of non-dissociatively adsorbed methanol [9]. The shoulder at 2970 cm^{-1} can be attributed to the asymmetric stretching mode $\nu_{as}(CH_3)$ of the methyl group in the methoxy species. Symmetric and asymmetric deformation vibration modes $\delta(CH_3)$ at 1433 and 1447 cm^{-1} as well as the rocking vibration mode $\rho(CH_3)$ at 1150 cm^{-1} detected in the low frequency region also correspond to the methoxy species [9]. In addition, the peaks assigned to the surface dioximethylene (CH_2O_2) species [50] were detected at 2923 and 2884 cm^{-1}. The spectrum obtained at 50 °C shows an intensive band

at 1627 cm^{-1} due to the bending mode of the adsorbed water molecules. Simultaneously, a strong peak was observed at 3400 cm^{-1} (not shown here) corresponding to the stretching vibration ν(OH) of adsorbed water and molecularly adsorbed methanol. Upon the temperature increasing from 50 to 120 °C, no significant changes were observed in the intensity of the vibration bands of the surface methoxy and dioximethylene species. Above 140 °C, the peaks at 1550, 1360, and 1655 cm^{-1} start to dominate. Two former peaks are characteristic of the ν_{as}(O-C-O) and ν_{s}(O-C-O) modes of the bidentate formate species and the feature at 1655 cm^{-1} is due to the stretching vibration ν(C=O) of adsorbed methyl formate [9,13,53]. The vibration frequencies are summarized in Table 3.

The methanol adsorption on the TiO_2 support was also investigated at the temperatures between 100 and 170 °C. Fig. 5 shows the typical FTIR spectrum of the adsorbed species on the pure TiO_2 (anatase) after the methanol adsorption at 100 °C. The intense peaks at 2960, 2925, 2831, and 1462 cm^{-1} correspond to the CH_3 stretching and bending modes of molecularly adsorbed methanol and methoxy species [9,13]. This is in a good agreement with low activity of TiO_2 in the methanol oxidation. No fingerprints of the adsorbed formaldehyde, dioximethylene, and formate species were detected between 100 and 170 °C.

3.4. In situ NAP XPS, XANES, and TPR study

Since *in situ* NAP XPS and XANES techniques can be used in the mbar pressure range [39,54-56], the correct comparison of the spectroscopic data with the kinetics measurements performed in the flow reactor at atmospheric pressure (Table 2 and Fig. 3) could be possible only if there is no pressure gap. The TPR technique was applied to verify this statement. The washed V_2O_5/TiO_2 catalyst was heated inside of the *in situ* XPS reaction gas cell in the equimolar CH_3OH/O_2 mixture and in clean methanol at total pressure of 0.25 mbar; the product distribution was monitored by a differentially pumped mass-spectrometer (Fig. 6). Priory, the catalyst was pretreated in 0.25 mbar of O_2 at 300 °C for 30 minutes.

The detection of formaldehyde and CO by a mass-spectrometer is hindered due to overlapping with the methanol fragmentation pattern. Nevertheless, the presence of formic acid,

methyl formate, and dimethoxymethane among the products was unambiguously proved by the m/z peaks of 45, 60, and 80, respectively. In the reaction mixture (Fig. 6a), the yield of DMM increases with the temperature increasing to 95 °C and then decreases. The MF yield shows a maximum as well; however, it appears at the higher temperature of *ca.* 130 °C. The FA production grows above 130 °C. A similar peak of DMM at 95 °C was also detected in the experiment with clean methanol (Fig. 6b); however, in the absence of O_2, the MF formation is suppressed and FA formation is facilitated above 130 °C. Therefore, catalytic behaviour in the mbar pressure range follows the same trends as under atmospheric pressure (Table 2, Fig. 3) and the results of *in situ* NAP XPS and XANES study are fully applicable. The NAP XPS and XANES spectra were also measured during heating the V_2O_5/TiO_2 catalyst in the step-wise manner both in the equimolar CH_3OH/O_2 mixture and in pure methanol.

The main NAP XPS results for the washed catalyst are summarized in Table 4. The V $2p_{3/2}$ and V $L_{2,3}$-edges XAS spectra along with the Ti $2p_{3/2}$ core level and Ti $L_{2,3}$-edges XAS spectra are shown in Fig. 7 and Fig. 8, respectively. Before the exposure to the reaction mixture, the catalyst was pretreated in 0.25 mbar of O_2 at 300 °C for 30 min inside of the *in situ* XPS reaction gas cell. This treatment led to the full vanadium oxidation: only a narrow single peak at 517.7 eV corresponding to the V^{5+} state was observed under oxygen atmosphere (Fig. 7a). A new V $2p_{3/2}$ peak at 516.4-516.5 eV appears in the reaction mixture pointing to the partial reduction of V^{5+} to V^{4+} even at room temperature. It should be noted that in the highly cited studies [57-61], vanadium ions in the vanadium oxides such as V_2O_5, V_2O_4, and V_2O_3 are characterized by the V $2p_{3/2}$ binding energy in the ranges of 516.9-517.2, 515.7-516.2, and 515.2-515.7 eV, respectively. However, the latest researches reported the higher binding energy values of V $2p_{3/2}$ at 517.3-517.7 and 516.2-516.5 eV, for bulk and supported V_2O_5, and for V_2O_4, respectively [20,62-68]. These numbers are in good agreement with our data.

Fig. 7b shows the V $L_{2,3}$-edges XAS spectra obtained during the same experiment. The transition energy and the line shape are sensitive to the chemical environment and can be used as a

fingerprint of a vanadium oxidation state [69,70]. Since the selection rules for the electron transition during photon absorption require $\Delta l = \pm 1$, therefore, the peaks at 518-519 and 524-525 eV in the XANES spectra presented in Fig. 7b can be roughly assigned to the electron excitations from the spin-orbit split levels $2p_{3/2}$ (L_3-edge) and $2p_{1/2}$ (L_2-edge) into the empty or partially occupied vanadium *3d* orbitals. The L_3-edge spectrum of the fully oxidized vanadia obtained in oxygen atmosphere shows the well-defined fine structure with at least four distinct resonances. The line shape is typical for V_2O_5 [70,71]. The position of the main resonance is 518.9 eV is also very close to the value of 519.1 eV reported for bulk V_2O_5 [70].

The treatment of the catalyst in the reaction mixture results in the shifting the V $L_{2,3}$-edge XAS spectrum towards lower energies and changing the line shape. To identify the fine structure, the difference XAS spectra were analyzed. Since according to the NAP XPS measurements (Table 4), only half of V^{5+} cations reduce to V^{4+} under the reaction conditions, the corresponding difference spectrum was obtained by subtracting the spectrum of the fully oxidized vanadia multiplied by 0.5 from the spectrum of the partially reduced vanadia (Fig. 7b). The difference L_3-edge spectrum is shifted towards lower energies and has another line shape. Only two distinct resonances are observed in the spectrum: the main resonance at 517.8 eV and well-distinguished shoulder at 515.9 eV. A similar line shape has been reported for bulk VO_2 [70,72,73]. Moreover, according to the correlation between the oxidation state and the L_3-edge peak position of binary vanadium oxides, this resonance corresponds to the V^{4+} state [74,75]. Indeed, Chen et al. [74] reported that the V L_3-edge position shifts by 0.7 eV per every ionic charge in the range from 515.5 eV (metallic vanadium) to 519.0 eV (V_2O_5). In current study, the shift is aproximatelly 0.8 eV that corresponds to the partial reduction of V^{5+} to V^{4+}. Thus, the XANES data proves the partial reduction of V^{5+} to V^{4+} under these reaction conditions.

No changes were detected in the Ti *2p* core-level and Ti *L*-edges XAS spectra under the reaction conditions from the room temperature to 200 °C. These data indicate that the support remains in the Ti^{4+} state. The narrow Ti $2p_{3/2}$ peaks with the full width at half maximum (FWHM)

of approximately 1.1 eV (Table 4) were at 459.0 eV, which is typical for bulk TiO_2 (Fig. 8a). According to the literature data [76-81], pure TiO_2 is characterized by the Ti $2p_{3/2}$ binding energy in the range of 458.7-459.2 eV, while the binding energy for the Ti^{3+} species is between 456.2 and 457.4 eV. The X-ray absorption spectra are shown in Fig. 8b. The spectra were normalized to the same maximum peak height. The spectra demonstrate the well-defined fine structure with at least seven distinct resonances. The main near-edge structure of the spectra is assigned to $2p^63d^0 \rightarrow 2p^5\underline{c}3d^1$ dipole transition, where $\underline{c}$ is for the $2p$ core hole [82]. Similar to vanadium, the $2p$ spin-orbit coupling splits the initial state into $2p_{3/2}$ and $2p_{1/2}$, resulting in two L-edge features, denoted as L_3 and L_2, respectively. Both the L_3 and L_2 features further split into the t_{2g} and e_{2g} components because of the low symmetry of the ligand field. The L_3-e_{2g} feature also splits into a doublet (peak D and E in the Fig. 8b) due to the slight distortion of the TiO_6 octahedron in the titania polymorphs that results from the configurational deformation predicted by the Jahn-Teller theorem [83]. The detailed description of the Ti L-edges spectra can be found elsewhere [84,85]. The different polymorphs of TiO_2 can be distinguished by the relative intensities of the D/E doublet [83,86,87]. For example, in the anatase structure, the intensity of the D peak is substantially stronger than the E peak intensity, whereas it is vice versa in the rutile structure. In the present study, all spectra shown in Fig. 8b are identical and their shape corresponds to the previously reported Ti L-edges spectra of anatase [83,86,87]. It means that during the methanol oxidation, the Ti^{4+} cations mainly are in the octahedral coordination in the TiO_2 anatase phase.

The results presented above clearly indicate that during the methanol oxidation the partial reduction of V^{5+} to V^{4+} occurs while the titanium cations remain in the Ti^{4+} state. The curve-fitting of the V $2p_{3/2}$ spectra (Fig. 7a) indicates that the relative contribution of the vanadium ions depends on the temperature; the quantitative data are presented in Table 4. Increasing the temperature from 100 to 200 °C decreases the V^{4+} fraction by more than 15 %. The catalyst reduces completely from V^{5+} to V^{4+} and V^{3+} following an exposure to methanol at 0.25 mbar even at the room temperature. This was concluded from the analysis of the V $2p_{3/2}$ spectra of the washed V_2O_5/TiO_2 catalysts

shown in Fig. 9. In methanol atmosphere, the typical V $2p_{3/2}$ spectrum of the fully oxidized V^{5+} catalyst with a single peak transforms into a spectrum with two peaks at 516.5-516.6 and 515.4-515.5 eV, which can be respectively attributed to V^{4+} and V^{3+}. The fraction of the V^{3+} state slightly grows with the temperature (Table 4). The subsequent treatment in oxygen at 300 °C leads again to the full oxidation of the reduced vanadium ions to V^{5+}. These data indicate that supported vanadium can undergo reversible oxidation and reduction during the methanol oxidation.

Fig. 10 shows the C*1s* core-level spectra measured *in situ* simultaneously with the V $2p_{3/2}$ and Ti $2p_{3/2}$ spectra. The oxygen treatment led to full removal of carbon from the catalyst surface. In a reaction mixture and in pure methanol the catalyst surface was covered by different carbon-contained species. In the reaction mixture (Fig. 10a), three components of the C *1s* spectrum could be distinguished at 285.3-285.4, 286.1-286.2, and 286.9-287.2 eV. The most intensive component at *ca.* 286.1 eV corresponds to methoxy species. The weaker component at *ca*. 285.0 eV is due to hydrocarbon impurities [4]. The third component at *ca.* 287.8 eV can be assigned both to gas phase methanol (the pressure is high enough to observe the gas phase signals [39,55]) and to molecularly chemisorbed methanol [4]. The amount of the methoxy species decreases with increasing of the temperature. A similar trend observed for the V^{4+} state (Table 4) indicates that the formation of the methoxy species on the vanadia surface is accompanied by the partial reduction of V^{5+} to V^{4+}. The C *1s* spectra obtained in pure methanol (Fig. 10b) contain an additional peak at 288.9 eV, which can be assigned to surface formate species. In this case, the significant fraction of vanadium is in the V^{3+} state (Table 4). The conclusion is that the formation of the formate species on the vanadia surface results in the partial reduction of V^{4+} to V^{3+}; however, the presence of oxygen leads to the fast re-oxidation of V^{3+} to V^{5+} (Fig. 10a).

4. Discussion

The catalytic and spectroscopic data obtained in this study confirm and clarify the detailed mechanism of the methanol oxidation over vanadia-titania catalysts proposed by Busca et al. [9-13].

The review of this mechanism can be found elsewhere [88]. The combined data of the *in situ* surface sensitive techniques, such as NAP XPS and XANES, with FTIR, TPR, and kinetics measurements allowed us to add into the reaction mechanism the changes of the vanadium chemical state. The proposed scheme is shown in Fig. 11.

Under mild conditions, dimethoxymethane and methyl formate are mainly produced on the V_2O_5/TiO_2 catalyst. The active sites of the methanol oxidation are associated with the highly dispersed vanadia supported on TiO_2. The absorption bands at 2955 and 2847 cm^{-1} at low temperatures (Fig. 4) indicate that the first step of the catalytic cycle is the methanol adsorption. Methanol chemically adsorbs by donating the electron density from the oxygen atom to the surface V^{5+} cation. The methanol adsorption through the hydrogen bonds with the surface hydroxyl groups and the lattice oxygen atoms also could not be ruled out. In the subsequent step, the adsorbed methanol dissociates to surface methoxy and hydroxyl groups, which was confirmed by FTIR (Fig. 4). The partial reduction of vanadium cations from the V^{5+} to V^{4+} state was detected by NAP XPS and XANES (Fig. 7). The methoxy species can be described as a monodentate structure with a covalent-type bond to the vanadium cation [9,48]. Due to the further loss of the hydrogen atom, the methoxy species transforms into the molecularly adsorbed formaldehyde and this is also accompanied by the partial reduction of the second vanadium cation from the V^{5+} to V^{4+} state. The hydroxyl groups recombine to produce water as a product.

Depending on the temperature, formaldehyde can desorbs as a product or undergoes the further transformation into the surface dioximethylene species. The dioximethylene species were also detected on the V_2O_5/TiO_2 catalyst by FTIR (Fig. 4). Since only minor amount of formaldehyde was detected in the gas phase by gas chromatography at 130 °C (Table 2) and a large amount of the surface dioximethylene species was observed during the formaldehyde oxidation on the same catalyst at 70 °C [50,89], the formation of the dioximethylene species from the adsorbed formaldehyde species should be a fast process.

The reaction of the dioximethylene species with methanol or methoxy species leads to dimethoxymethane, which is the main reaction product at the low temperatures (Table 2). Most likely, this reaction proceeds through the nucleophilic attack of the dioximethylene carbon atom by oxygen from two adjacent methoxy species or from adsorbed methanol molecules [90]. It is confirmed by that up to 120 °C, DMM was produced with a high selectivity and the surface was covered with the dioximethylene species, molecularly adsorbed methanol, and the methoxy species as shown in Fig. 4.

At higher temperatures, dioximethylene is oxidized into the formate species. The formation of the formate species is accompanied by the reduction of vanadium cations to the V^{3+} state which was observed by XPS in methanol atmosphere (Fig. 8). In methanol/oxygen mixture, the V^{3+} cation was not detected because re-oxidation of V^{3+} to V^{4+} and/or V^{5+} is a fast process in the presence of gas phase oxygen. The formate species can transform into formic acid and carbon oxide [9] or react with methanol resulting in methyl formate. This was confirmed by FTIR showing that the concentration of the dioximethylene species decreases above 120 °C, whereas the intensities of the bands at 1550 and 1360 cm^{-1} (the stretching vibrations of the formate species) and the band at 1655 cm^{-1} (adsorbed methyl formate) increase (Fig. 4). In good agreement with this mechanism, the V_2O_5/TiO_2 catalysts demonstrated high selectivity in the formaldehyde oxidation to formic acid under similar conditions [34,50,89]. It was shown recently that the formate species is stable up to 180 °C in helium but readily decomposes in oxygen at 100-150 °C resulting in the formation of formic acid [50]. A similar behavior was observed in the present *in situ* XPS study. Indeed, the formate species were identified in the C *1s* spectra measured in the methanol flow (Fig. 10b), whereas the oxygen presence in the reaction mixture leads to decreasing the concentration of the adsorbed formate species below the XPS sensitivity limit (Fig. 10a). As a result, the formation of formic acid was observed in the TPR experiments (Fig. 6).

Re-oxidation of the vanadium active sites by dioxygen completes the catalytic cycle. Although it is difficult to explain how O_2 molecule is transformed to the lattice O^{2-} species in the

case of the monolayer V_2O_5/TiO_2 catalyst, re-oxidation of V^{3+} and V^{4+} to V^{5+} during the methanol oxidation in the presence of O_2 in the gas phase was clearly observed by XPS (Fig. 7 and 8, Table 4). It should be underlined that the re-oxidation of the catalyst surface should restore its adsorption properties because methanol mainly adsorbs on V^{5+} sites. From this point of view, the fully oxidized vanadia should be more active than partially reduced one. This hypothesis is confirmed by the fact that the methanol conversion on the V-Ti oxide catalyst at 175 °C gradually decreases from 100 to aproximatelly 30 % upon increasing the molar methanol/oxygen ratio from 0.5 to 2.7 [9,11]. This is in agreement with the data by Wang and Madix [91], who have shown that the fully oxidized surface in a model monolayer $V_2O_5/TiO_2(110)$ catalyst has a much higher activity in the methanol oxidation to formaldehyde than the reduced surface with the vanadium oxidation states of V^{3+} and V^{4+}.

The presented data are in line with the proposal that the selective oxidation of methanol on the monolayer V_2O_5/TiO_2 catalyst occurs at the redox V^{n+} sites through the Mars-van Krevelen mechanism [92] involving the lattice oxygen species (see the proposed scheme in Fig.11). Final proof of this mechanism will require the comparison of the methanol oxidation rate over the V_2O_5/TiO_2 catalyst in the presence and in the absence of oxygen [93] and is the subject of a future work.

5. Conclusions

It has been shown that the highly dispersed vanadia supported on TiO_2 is an active and selective catalyst for the oxidation of methanol to methyl formate and dimethoxymethane under mild conditions. At the low temperatures (70-100ºC), dimethoxymethane is the main reaction product with the selectivity of 88-95 %, whereas at the higher temperatures (150ºC), methyl formate becomes the main reaction product with the selectivity of 85 %. The production of formaldehyde is greatly inhibited in this temperature range. Inverse dependence of the selectivity and the product

formation rates indicates that methyl formate forms through successive dimethoxymethane transformation.

Combination of the catalytic measurements with *in situ* FTIR, NAP XPS, XANES, and TPR provided the additional insight into the mechanism of the methanol oxidation. FTIR showed the presence of the non-dissociatively adsorbed molecules of methanol as well as the adsorbed methoxy, dioximethylene, and formate species. NAP XPS and XANES demonstrated that the reaction involves the reversible reduction of V^{5+} cations. This proved that the lattice oxygen takes part in the methanol oxidation via the classical Mars-van Krevelen mechanism. This mechanism consists of the reduction of the catalyst surface by methanol and its subsequent re-oxidation by oxygen from the gas phase. The reaction starts from the molecular chemisorption of methanol on the V^{5+} cations. The following dissociation of the adsorbed molecules to methoxy species and hydroxyl groups is accompanied by the reduction of the vanadium cations from the V^{5+} to V^{4+} state. The oxidation (H abstraction and electron transfer) of the methoxy species leads to the formation of adsorbed formaldehyde, which can desorb as the product or can transform into the surface dioximethylene species. The reaction of the dioximethylene species with methanol or the methoxy species leads to dimethoxymethane, which is the main product at low temperatures. At higher temperatures, dioximethylene transforms into the formate species, which can also react with methanol resulting in methyl formate. The formation of the formate species is accompanied by the reduction of vanadium to V^{3+}. The catalytic cycle is completed by re-oxidition of the vanadium cations again to the V^{5+} state by molecular oxygen from the gas phase.

Acknowledgments

This work was partially supported through the Integrated Infrastructure Initiative I3 in FP6 R II 3 CT-2004-506008 (BESSY IA-SFS Access Program) and by RFBR (Research project No. 13-03-00128). The authors gratefully thank M. Hävecker, E. Kleimenov, D. Tescher, S. Zafeiratos for their help in carrying out ambient pressure XPS and XANES measurements as well as the staff of

BESSY for their support in beamline operation. The authors are also grateful to L.M. Plyasova for XRD measurements.

References

[1] J.M. Tatibouët, Appl. Catal. A 148 (1997) 213.

[2] P. Forzatti, E. Tronconi, A.S. Elmi, G. Busca, Appl. Catal. A 157 (1997) 387.

[3] M. Badlani, I.E. Wachs, Catal. Lett. 75 (2001) 137.

[4] Y. Romanyshyn, S. Guimond, H. Kuhlenbeck, S. Kaya, R.P. Blum, H. Niehus, S. Shaikhutdinov, V. Simic-Milosevic, N. Nilius, H.-J. Freund, M.V. Ganduglia-Pirovano, R. Fortrie, J. Döbler, J. Sauer, Top. Catal. 50 (2008) 106.

[5] J.M. Tatibuet, J.E. Germain, C.R. Acad. Sci. C 289 (1979) 305.

[6] M. Baltes, K. Cassiers, P.v.D. Voort, B.M. Weckhuysen, R.A. Schoonheydt, E.F. Vansant, J. Catal. 197 (2001) 160.

[7] C. Hess, I.J. Drake, J.D. Hoefelmeyer, T.D. Tilley, A.T. Bell, Catal. Lett. 105 (2005) 1.

[8] N. Koivikko, T. Laitinen, S. Ojala, S. Pitkäaho, A. Kucherov, R.L. Keiski, Appl. Catal. B 103 (2001) 72.

[9] G. Busca, A.S. Elmi, P. Forzatti, J. Phys. Chem. 91 (1987) 5263.

[10] P. Forzatti, E. Tronconi, G. Busca, P. Tittarelli, Catal. Today 1987 (1987) 209.

[11] E. Tronconi, A.S. Elmi, N. Ferlazzo, P. Forzatti, G. Busca, Ind. Eng. Chem. Res. 26 (1987) 1269.

[12] A.S. Elmi, E. Tronconi, C. Cristiani, J.P.G. Martin, P. Forzatti, G. Busca, Ind. Eng. Chem. Res. 28 (1989) 387.

[13] G. Busca, J. Mol. Catal. 50 (1989) 241.

[14] Y. Fu, J. Shen, Chem. Commun. (2007) 2172.

[15] Q. Sun, Y. Fu, J. Liu, A. Auroux, J. Shen, Appl. Catal. A 334 (2008) 26.

[16] J. Liu, Y. Fu, Q. Sun, J. Shen, Micropor. Mesopor. Mater. 116 (2008) 614.

[17] J. Liu, Q. Sun, Y. Fu, J. Shen, J. Colloid Interf. Sci. 335 (2009) 216.

[18] H. Zhao, S. Bennici, J. Shen, A. Auroux, J. Mol. Catal. A 309 (2009) 28.

[19] H. Zhao, S. Bennici, J. Shen, A. Auroux, J. Catal. 272 (2010) 176.

[20] H. Zhao, S. Bennici, J. Cai, J. Shen, A. Auroux, Catal. Today 152 (2010) 70.

[21] Q. Sun, J. Liu, J. Cai, Y. Fu, J. Shen, Catal. Commun. 11 (2010) 47.

[22] H. Guo, D. Li, D. Jiang, W. Li, Y. Sun, Catal. Commun. 11 (2010) 396.

[23] J.S. Lee, J.C. Kim, Y.G. Kim, Appl. Catal. A 57 (1990) 1.

[24] G. Jenner, Appl. Catal. A 121 (1995) 25.

[25] Q. Sun, A. Auroux, J. Shen, J. Catal. 244 (2006) 1.

[26] Y. Fu, J. Shen, J. Catal. 248 (2007) 101.

[27] G.C. Bond, J.P. Zurita, S. Flamerz, P.J. Gellings, H. Bosch, J.G. van Ommen, B.J. Kip, Appl. Catal. 22 (1986) 361.

[28] D.A. Bulushev, L. Kiwi-Minsker, F. Rainone, A. Renken, J. Catal. 205 (2002) 115.

[29] G.C. Bond, S.F. Tahir, Appl. Catal. A 71 (1991) 1.

[30] G. Deo, I.E. Wachs, J. Catal. 146 (1994) 323.

[31] I.E. Wachs, Catal. Today 27 (1996) 437.

[32] I.E. Wachs, B.M. Weckhuysen, Appl. Catal. A 157 (1997) 67.

[33] B. Grzybowska-Swierkosz, Appl. Catal. A 157 (1997) 263.

[34] G.Y. Popova, T.V. Andrushkevich, E.V. Semionova, Y.A. Chesalov, L.S. Dovlitova, V.A. Rogov, V.N. Parmon, J. Mol. Catal. A 283 (2007) 146.

[35] M.V. Martinez-Huerta, J.L.G. Fierro, M.A. Banares, Catal. Commun. 11 (2009) 15.

[36] I.E. Wachs, R.Y. Saleh, S.S. Chan, C.C. Chersich, Appl. Catal. 15 (1985) 339.

[37] E.V. Kondratenko, M. Baerns, Appl. Catal. A 222 (2001) 133.

[38] E.V. Ovchinnikova, T.V. Andrushkevich, G.Y. Popova, V.D. Meshcheryakov, V.A. Chumachenko, Chem. Eng. J. 154 (2009) 60.

[39] A. Knop-Gericke, E. Kleimenov, M. Hävecker, R. Blume, D. Teschner, S. Zafeiratos, R. Schlögl, V.I. Bukhtiyarov, V.V. Kaichev, I.P. Prosvirin, A.I. Nizovskii, H. Bluhm, A. Barinov, P. Dudin, M. Kiskinova, Adv. Catal. 52 (2009) 213.

[40] G.C. Bond, A. Sarkany, G.D. Parfitt, J. Catal. 57 (1979) 476.

[41] B.M. Reddy, I. Ganesh, B. Chowdhury, Catal. Today 49 (1999) 115.

[42] G. Busca, A. Zecchina, Catal. Today 20 (1994) 61.

[43] B.P. Barbero, L.E. Cadus, Appl. Catal. A 244 (2003) 235.

[44] V. Dimitrov, Y. Dimitriev, A. Montenero, J. Non-Crystall. Solids 244 (1994) 235.

[45] E.V. Danilevich, G.Y. Popova, T.V. Andrushkevich, Y.A. Chesalov, V.V. Kaichev, A.A. Saraev, L.M. Plyasova, Stud. Surf. Sci. Catal. 175 (2010) 463.

[46] F. Roozeboom, P.D. Cordingley, P.J. Gellings, J. Catal. 68 (1981) 464.

[47] G. Busca, V. Lorenzelli, J. Catal. 66 (1980) 155.

[48] G. Busca, P.F. Rossi, V. Lorenzelli, M. Benoissa, J. Travert, J.C. Lavalley, J. Phys. Chem. 89 (1985) 5433.

[49] L.J. Burcham, I.E. Wachs, Catal. Today 49 (1999) 467.

[50] G.Y. Popova, Y.A. Chesalov, T.V. Andrushkevich, E.S. Stoyanov, Kinet. Catal. 41 (2000). 546.

[51] L.J. Burcham, L.E. Briand, I.E. Wachs, Langmuir 17 (2001) 6164.

[52] L.J. Burcham, M. Badlani, I.E. Wachs, J. Catal. 203 (2001) 104.

[53] V. Lochar, J. Machek, J. Tichy, Appl. Catal. A 228 (2002) 95.

[54] A. Knop-Gericke, M. Hävecker, Th. Schedel-Niedrig, R. Schlögl, Top. Catal. 10 (2000) 187.

[55] V.I. Bukhtiyarov, V.V. Kaichev, I.P. Prosvirin, Top. Catal. 32 (2005) 3.

[56] V.V. Kaichev, A.V. Miller, I.P. Prosvirin, V.I. Bukhtiyarov, Surf. Sci. 606 (2012) 420.

[57] R.J. Colton, A.M. Guzman, J.W. Rabalais, J. Appl. Phys. 49 (1978) 409.

[58] G.A. Sawatzky, D. Post, Phys. Rev. B 20 (1979) 1546.

[59] J. Mendialdua, R. Casanova, Y. Barbaux, J. Electron Spectrosc. Relat. Phenom. 71 (1995) 249.

[60] M. Demeter, M. Neumann, W. Reichelt, Surf. Sci. 454-456 (2000) 41.

[61] G. Silversmit, D. Depla, H. Poelman, G.B. Marin, R.D. Cryse, J. Electron Spectrosc. Relat. Phenom. 135 (2004) 167.

[62] M. Sambi, G. Sangiovanni, G. Granozzi, F. Parmigiani, Phys. Rev. B 55 (1997) 7580.

[63] M.E. Harlin, V.M. Niemi, A.O.I. Krause, J. Catal. 195 (2000) 67.

[64] K.V.R. Chary, G. Kishan, C.P. Kumar, G.V. Sagar, J.W. Niemantsverdriet, Appl. Catal. A 245 (2003) 303.

[65] L.K. Boudali, A. Ghorbel, P. Grage, F. Figueras, Appl. Catal. B 59 (2005) 105.

[66] J. Haber, Catal. Today 142 (2009) 100.

[67] Z. Wu, F. Dong, Y. Liu, H. Wang, Catal. Commun. 11 (2009) 82.

[68] Q. Tang, Y. Chen, Y. Yang, J. Mol. Catal. A 315 (2010) 43.

[69] J. Biener, M. Bäumer, R.J. Madix, P. Liu, E.J. Nelson, T. Kendelewicz, G.E.B. Jr., Surf. Sci. 441 (1999) 1.

[70] R. Zimmermann, R. Claessen, F. Reinert, P. Steiner, S. Hüfner, J. Phys.: Condens. Matter 10 (1998) 5697.

[71] M. Hävecker, A. Knop-Gericke, R.W. Mayer, M. Fait, H. Bluhm, R. Schlögl, J. Electron Spectrosc. Relat. Phenom. 125 (2001) 79.

[72] M. Abbate, F.M.F.d. Groot, J.C. Fuggle, Y.J. Ma, C.T. Chen, F. Sette, A. Fujimori, Y. Ueda, K. Kosuge, Phys. Rev. B 43 (1991) 7263.

[73] D. Ruzmetov, S.D. Senanayake, S. Ramanathan, Phys. Rev. B 75 (2007) 195102.

[74] J.G. Chen, C.M. Kirn, B. Frühberger, B.D. DeVries, M.S. Touvelle, Surf. Sci. 321 (1995) 145.

[75] D.S. Su, V. Roddatis, M. Willinger, G. Weinberg, E. Kitzelmann, R. Schlögl, H. Knözinger, Catal. Lett. 74 (2001) 169.

[76] C.M. Greenlief, J.M. White, C.S. Ko, R.J. Gorte, J. Phys. Chem. 89 (1985) 5025.

[77] A.Y. Stakheev, E.S. Shpiro, J. Apijok, J. Phys. Chem. 97 (1993) 5668.

[78] R. Sanjines, H. Tang, H. Berger, F. Gozzo, G. Margaritondo, F. Levy, J. Appl. Phys. 75 (1994) 2945.

[79] Z. Luan, E.M. Maes, P.A.W.v.d. Heide, D. Zhao, R.S. Czernuszewicz, L. Kevan, Chem. Mater. 11 (1999) 3680.

[80] Y. Hasegawa, A. Ayame, Catal. Today 71 (2001) 177.

[81] P. Finetti, F. Sedona, G.A. Rizzi, U. Mick, F. Sutara, M. Svec, V. Matolin, K. Schierbaum, G. Granozzi, J. Phys. Chem. C 111 (2007) 869.

[82] C.Heiliger, F. Heyroth, F. Syrowatka, H.S. Leipner, I. Maznichenko, K. Kokko, W. Hergert, I. Mertig, Phys. Rev. B 73 (2006) 045129.

[83] R. Brydson, H. Sauer, W. Engel, J.M. Thomas, E. Zeitler, N. Kosugi, H. Kuroda, J. Phys.: Condens. Matter 1 (1989) 797.

[84] J.G. Chen, Surf. Sci. Rep. 30 (1997) 1.

[85] H.C. Choi, H.-J. Ahn, Y.M. Jung, M.K. Lee, H.J. Shin, S.B. Kim, Y.-E. Sung, Appl. Spectrosc. 58 (2004) 598.

[86] J.P. Crocombette, F. Jollet, J. Phys.: Condens. Matter 6 (1994) 10811.

[87] E. Stoyanov, F. Langenhorst, G. Steinle-Neumann, Am. Mineral. 92 (2007) 577.

[88] G. Centi, F. Cavani, F. Trifiro, Selective oxidation by heterogeneous catalysis, Kluwer Academic/Plenum Publishers, New York, 2001, p. 143.

[89] G.Y. Popova, Y.A. Chesalov, T.V. Andrushkevich, I.I. Zakharov, E.S. Stoyanov, J. Mol. Catal. A 158 (2000) 345.

[90] Y.C. Liu, G.L. Griffin, S.S. Chan, I.E. Wachs, J. Catal. 94 (1985) 108.

[91] Q. Wang, R.J. Madix, Surf. Sci. 496 (2002) 51.

[92] P. Mars, D.W. van Krevelen, Chem. Eng. Sci. 3 (1954) 41.

[93] G.Y. Popova, T.V. Andrushkevich, Y.A. Chesalov, V.N. Parmon, J. Mol. Catal. A 268 (2007) 251.

Figure Captions

Fig. 1. X-ray diffraction patterns obtained from TiO_2 anatase (1), fresh (2) and washed (3) V_2O_5/TiO_2 catalysts. The marked features are from V_2O_5.

Fig. 2. FTIR spectra of TiO_2 anatase (1), fresh (2) and washed (3) V_2O_5/TiO_2 catalysts, bulk V_2O_5 (4) after calcination at 400 °C in the air flow, as well as difference spectra (2-1 and 3-1), which are obtained by direct subtraction of spectrum 1 from spectra 2 and 3, respectively.

Fig. 3. Effect of reaction temperature on rate ($10^{-9} \cdot mol \cdot m^{-2} \cdot s^{-1}$) of dimethoxymethane (a), methyl formate (b), formaldehyde (c), formic acid (d), and CO_x (e) formation (right side) and its selectivity (left side). Conversion of methanol is 50 %.

Fig. 4. FTIR difference spectra of the washed V_2O_5/TiO_2 catalyst obtained during the methanol oxidation at different temperatures: 1 – 50 °C, 2 – 100 °C, 3 – 120 °C, 4 – 140 °C, 5 – 160 °C, 6 – 180 °C.

Fig. 5. FTIR difference spectra of TiO_2 (anatase) obtained during the methanol absorption at 100 °C.

Fig. 6. TPR spectra measured in the equimolar CH_3OH/O_2 mixture (a) and in methanol (b) with total pressure of 0.25 mbar.

Fig. 7. Normalized V $2p_{3/2}$ core-level spectra (a) and V $L_{2,3}$-edges XAS spectra (b) of the washed V_2O_5/TiO_2 catalyst measured in 0.25 mbar O_2 at 300 °C (1) as well as in the equimolar CH_3OH/O_2 mixture with total pressure of 0.25 mbar at 100, 150, and 200 °C (2, 3, 4); 2-1 is difference XAS spectrum obtained by direct subtraction of spectrum 1 multiplied on factor 0.5 from spectrum 2, respectively.

Fig. 8. Normalized Ti $2p_{3/2}$ core-level spectra (a) and Ti $L_{2,3}$-edge XAS spectra (b) of the washed V_2O_5/TiO_2 catalyst measured in 0.25 mbar O_2 at 300 °C (1) as well as in the equimolar CH_3OH/O_2 mixture with total pressure of 0.25 mbar at 100, 150, and 200 °C (2, 3, 4), respectively.

Fig. 9. Normalized V $2p_{3/2}$ core-level spectra of the washed V_2O_5/TiO_2 catalyst measured in 0.25 mbar O_2 at 300 °C (1) as well as in 0.25 mbar CH_3OH at 50, 100, 150, and 200 °C (2, 3, 4, 5), respectively.

Fig. 10. The C *1s* core-level spectra of the washed V_2O_5/TiO_2 catalyst measured in 0.25 mbar O_2 at 300 °C (1) as well as in an equimolar CH_3OH/O_2 mixture (a) and in pure CH_3OH (b) at 100, 150, and 200 °C (2, 3, 4), respectively; total pressure of 0.25 mbar; the V *2p* integral intensity was normalized for all spectra.

Fig. 11. Proposed mechanism for methanol oxidation on highly dispersed vanadia supported on TiO_2.

Table Captions

Table 1 Characteristics of the fresh and washed V_2O_5/TiO_2 catalysts.

Table 2 Catalytic properties of the washed V_2O_5/TiO_2 catalyst in the methanol oxidation. [a]

Table 3 IR bands and assignments of the surface species formed in the methanol oxidation on the V_2O_5/TiO_2 catalyst.

Table 4 Binding energies and FWHMs of the Ti $2p_{3/2}$ and V $2p_{3/2}$ peaks shown in Figs. 7a, 8a, and 9; the relative intensity of different components (%) shown in parentheses.

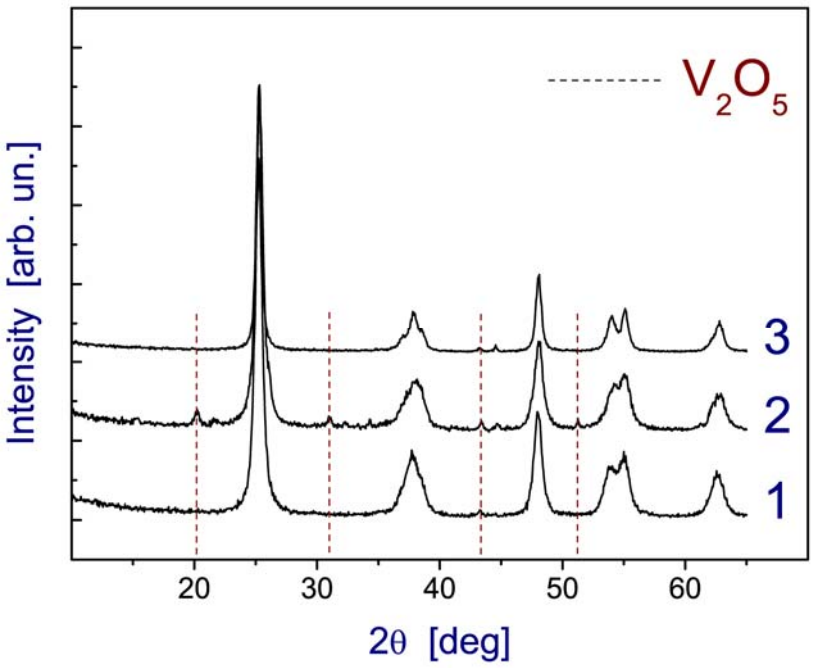

Fig. 1. X-ray diffraction patterns obtained from TiO_2 anatase (1), fresh (2) and washed (3) V_2O_5/TiO_2 catalysts. The marked features are from V_2O_5.

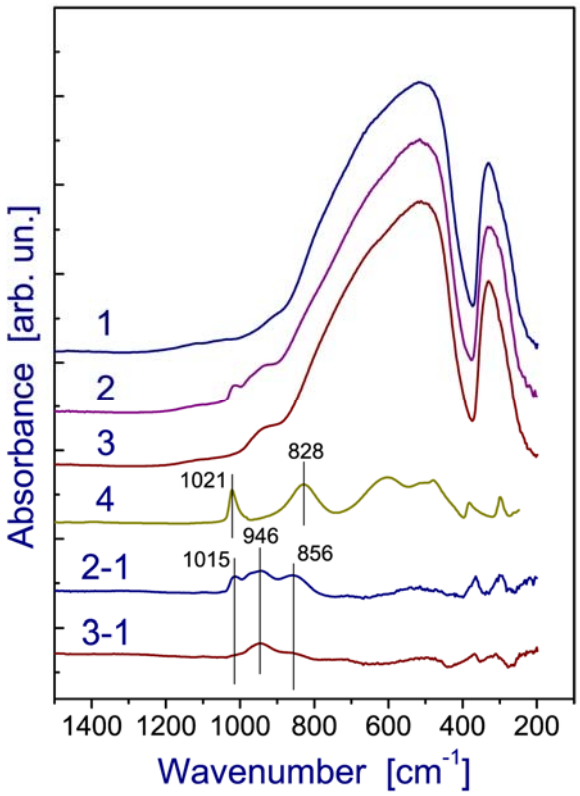

Fig. 2. FTIR spectra of TiO_2 anatase (1), fresh (2) and washed (3) V_2O_5/TiO_2 catalysts, bulk V_2O_5 (4) after calcination at 400 °C in the air flow, as well as difference spectra (2-1 and 3-1), which are obtained by direct subtraction of spectrum 1 from spectra 2 and 3, respectively.

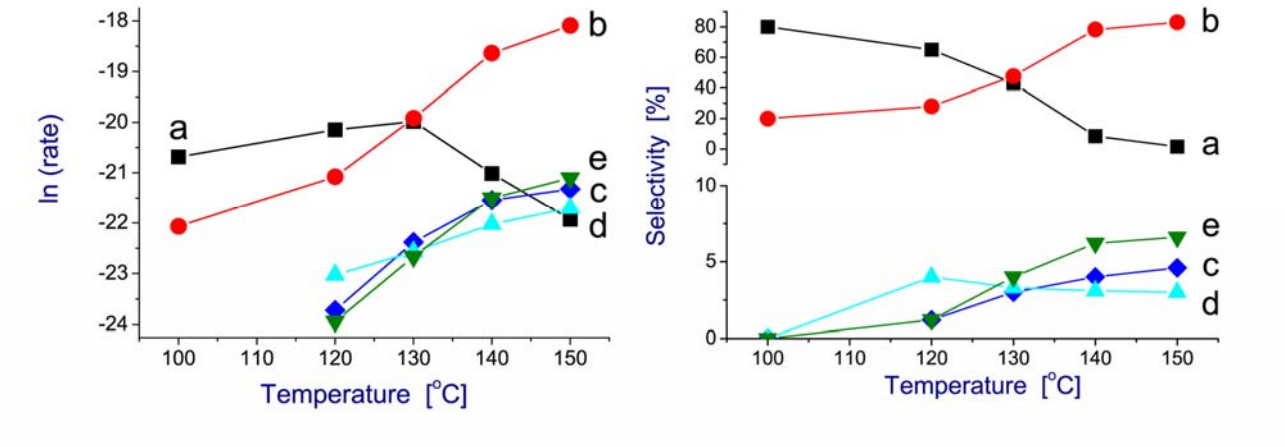

Fig. 3. Effect of reaction temperature on rate ($10^{-9} \cdot mol \cdot m^{-2} \cdot s^{-1}$) of dimethoxymethane (a), methyl formate (b), formaldehyde (c), formic acid (d), and CO_x (e) formation (right side) and its selectivity (left side). Conversion of methanol is 50 %.

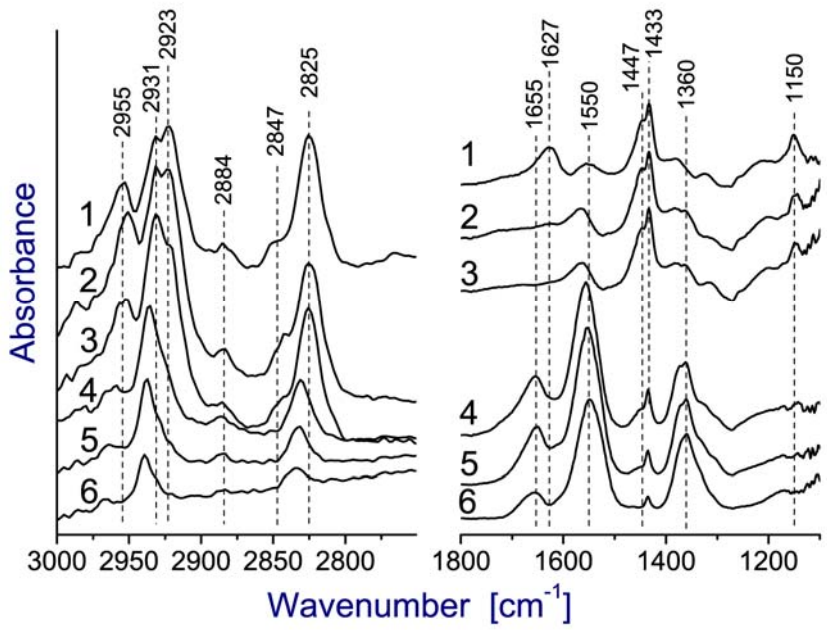

Fig. 4. FTIR difference spectra of the washed V_2O_5/TiO_2 catalyst obtained during the methanol oxidation at different temperatures: 1 – 50 °C, 2 – 100 °C, 3 – 120 °C, 4 – 140 °C, 5 – 160 °C, 6 – 180 °C.

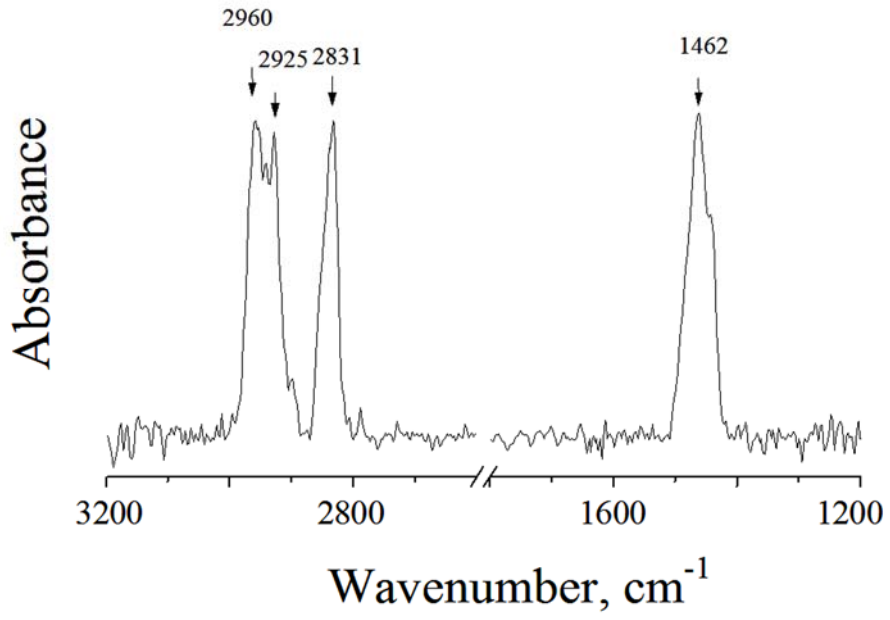

Fig. 5. FTIR difference spectra of TiO_2 (anatase) obtained during the methanol absorption at 100 °C.

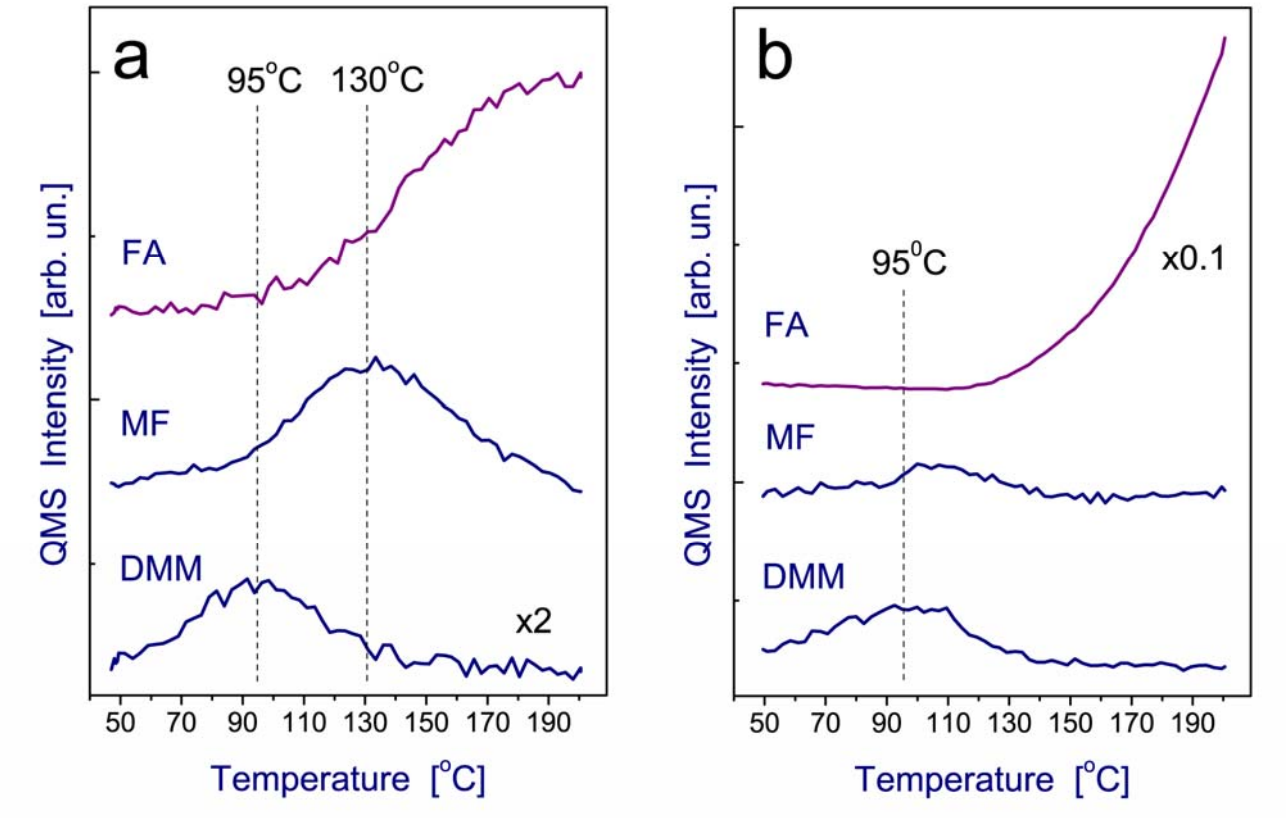

Fig. 6. TPR spectra measured in the equimolar CH_3OH/O_2 mixture (a) and in methanol (b) with total pressure of 0.25 mbar.

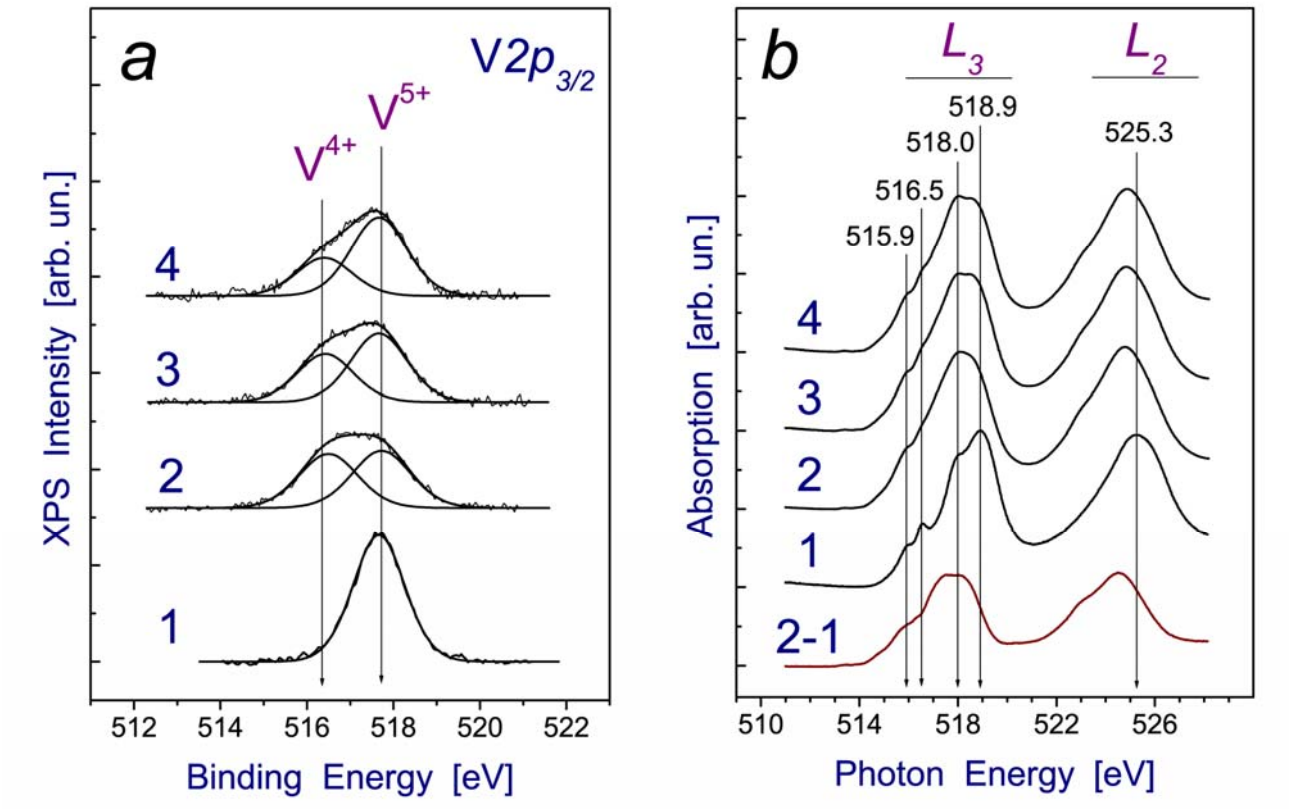

Fig. 7. Normalized V $2p_{3/2}$ core-level spectra (a) and V $L_{2,3}$-edges XAS spectra (b) of the washed V_2O_5/TiO_2 catalyst measured in 0.25 mbar O_2 at 300 °C (1) as well as in the equimolar CH_3OH/O_2 mixture with total pressure of 0.25 mbar at 100, 150, and 200 °C (2, 3, 4); 2-1 is difference XAS spectrum obtained by direct subtraction of spectrum 1 multiplied on factor 0.5 from spectrum 2, respectively.

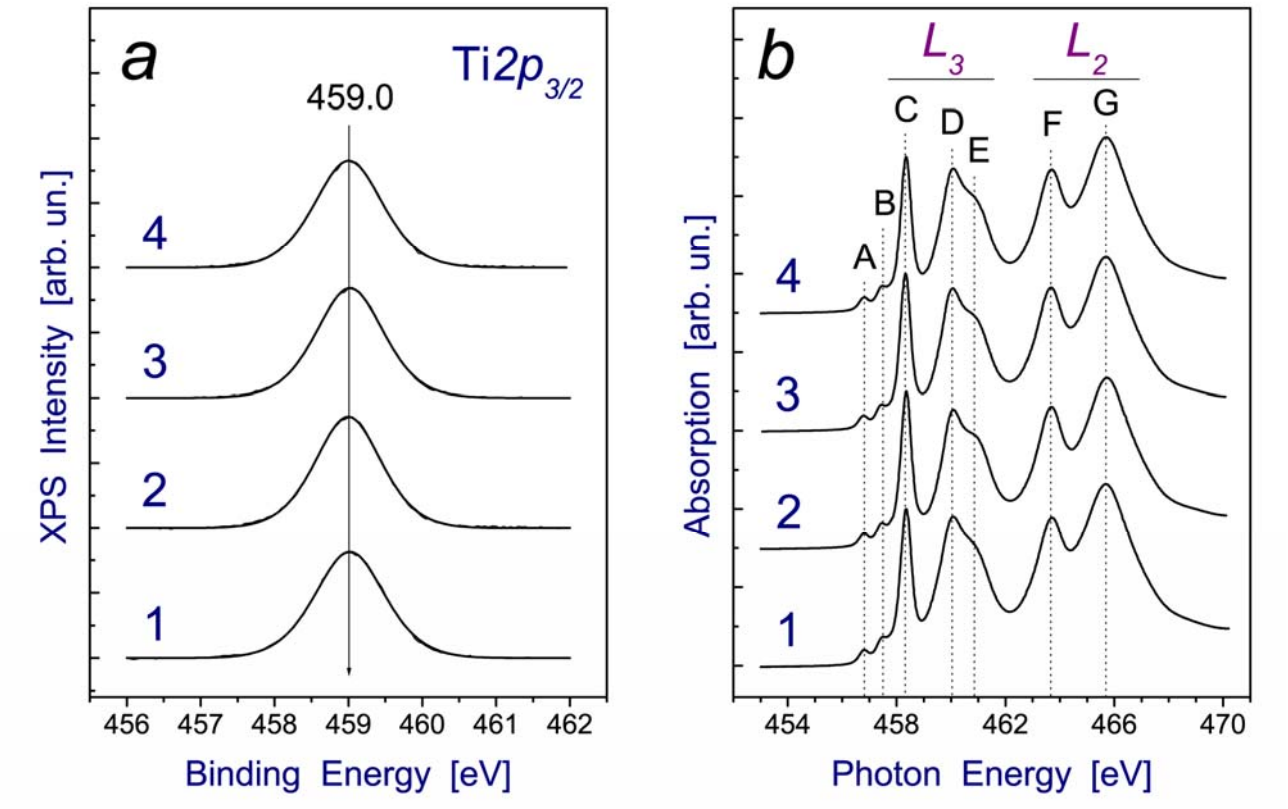

Fig. 8. Normalized Ti $2p_{3/2}$ core-level spectra (a) and Ti $L_{2,3}$-edge XAS spectra (b) of the washed V_2O_5/TiO_2 catalyst measured in 0.25 mbar O_2 at 300 °C (1) as well as in the equimolar CH_3OH/O_2 mixture with total pressure of 0.25 mbar at 100, 150, and 200 °C (2, 3, 4), respectively.

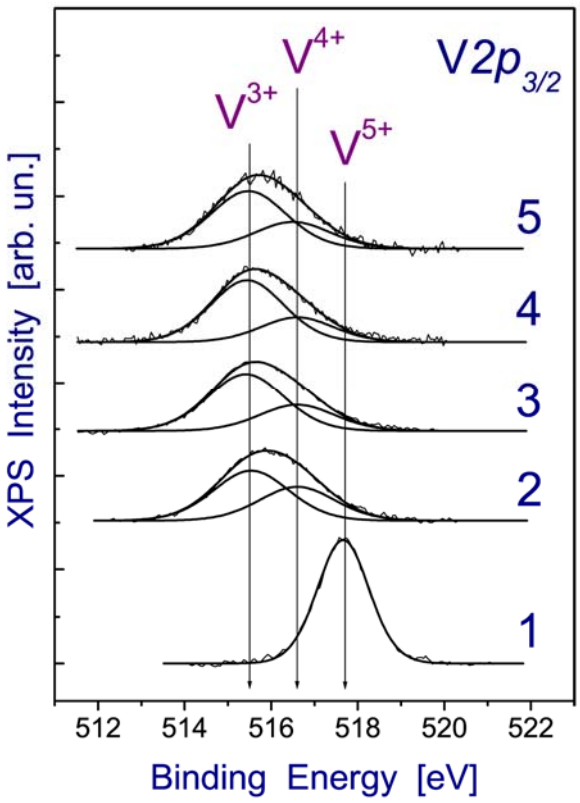

Fig. 9. Normalized V *2p*$_{3/2}$ core-level spectra of the washed V_2O_5/TiO_2 catalyst measured in 0.25 mbar O_2 at 300 °C (1) as well as in 0.25 mbar CH_3OH at 50, 100, 150, and 200 °C (2, 3, 4, 5), respectively.

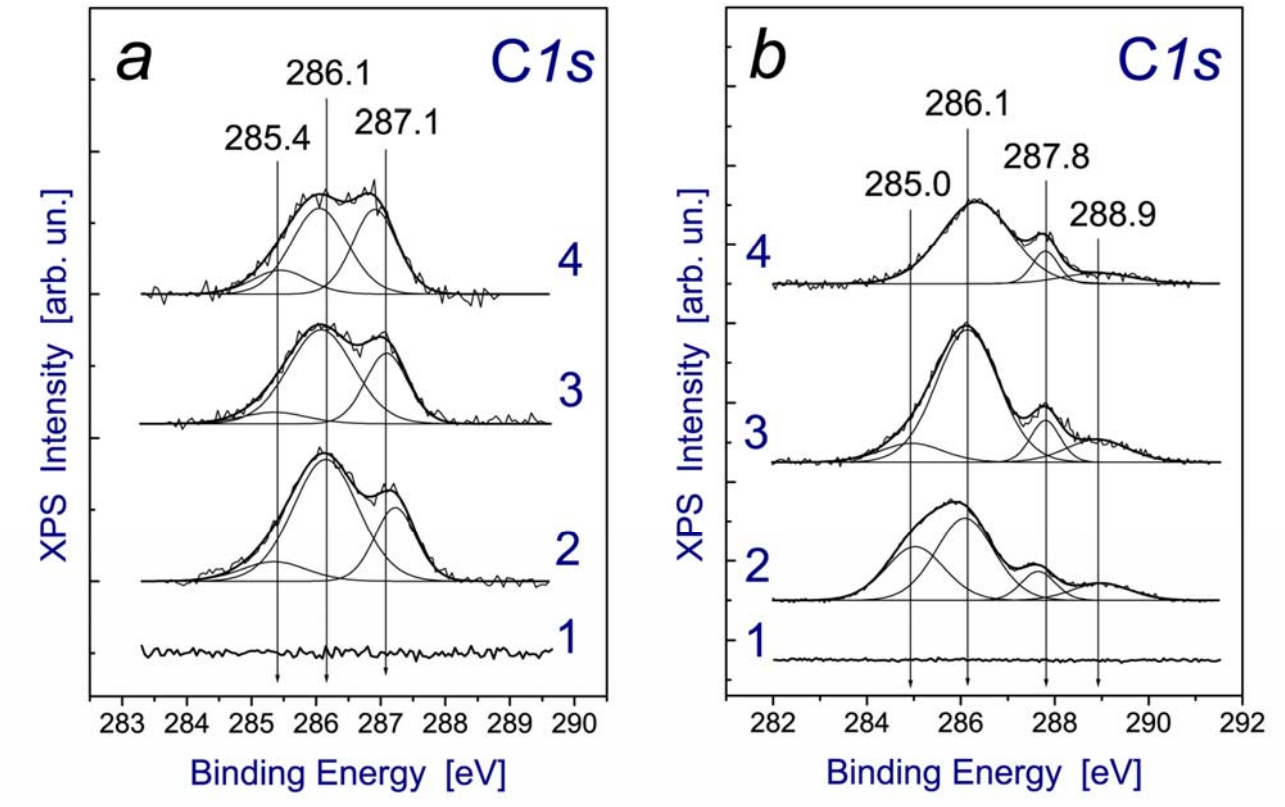

Fig. 10. The C *1s* core-level spectra of the washed V_2O_5/TiO_2 catalyst measured in 0.25 mbar O_2 at 300 °C (1) as well as in an equimolar CH_3OH/O_2 mixture (a) and in pure CH_3OH (b) at 100, 150, and 200 °C (2, 3, 4), respectively; total pressure of 0.25 mbar; the V *2p* integral intensity was normalized for all spectra.

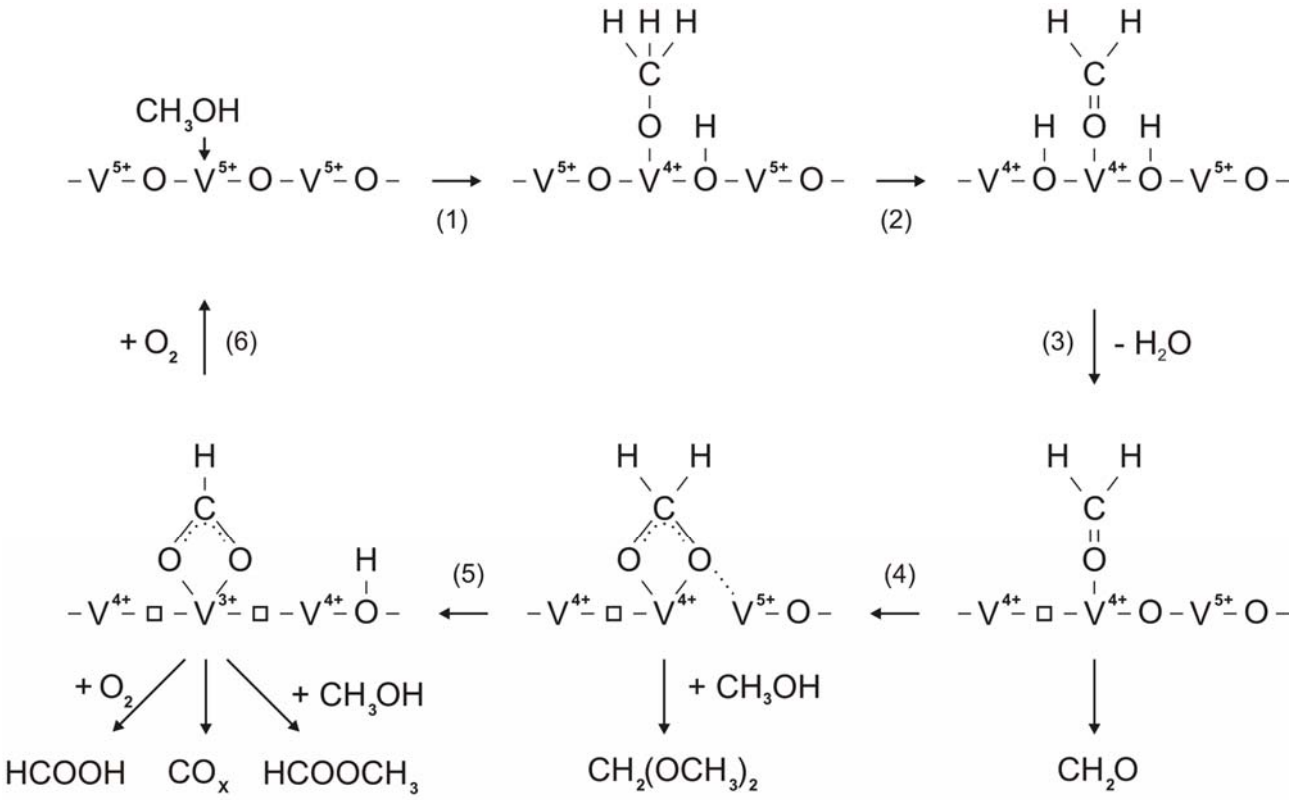

Fig. 11. Proposed mechanism for methanol oxidation on highly dispersed vanadia supported on TiO_2.

Table 1

Characteristics of the fresh and washed V_2O_5/TiO_2 catalysts.

Catalyst	V_2O_5 content, wt%	S_{BET}, m^2/g	V_2O_5 surface density[a], V-atom/nm^2	V_2O_5 surface coverage[b], ML
Fresh	20	111	11.9	1.5
washed	12.5	115	7.3	0.9

[a] Referred to the BET area.

[b] 1 ML corresponds to 7.9 V-atom/nm^2 [31].

Table 2

Catalytic properties of the washed V_2O_5/TiO_2 catalyst in the methanol oxidation. [a]

Temp,	Catalyst	Feed flow,	Conversion,	Selectivity, %					
ºC	load, g	l/h	%	DMM	MF	F	FA	CO	CO_2
70	2.0	2.5	10.0	95	5.0	0	0	0	0
100	2.0	2.5	17.0	90	10.0	0	0	0	0
120	**2.0**	**2.5**	**30.1**	**75**	**19.4**	**2.5**	**3.1**	**0**	**0**
130	2.0	2.5	44.0	43	46.7	4.0	2.3	3.0	1.0
140	2.0	2.5	60.0	3	83.9	3.6	2.5	5.5	1.5
100	2.0	4.5	10.0	94	6.0	0	0	0	0
120	**2.0**	**4.5**	**20.5**	**80**	**17.0**	**3**	**0**	**0**	**0**
140	2.0	4.5	45.0	8.2	78.5	5.0	3.1	4.1	1.1
100	7.5	2.5	45.0	80	20.0	0	0	0	0
120	**7.5**	**2.5**	**59.7**	**57**	**32.8**	**2.0**	**5.1**	**3.1**	**0**
130	7.5	2.5	73.5	15	74.5	2.5	4.0	4.0	0.0
140	7.5	2.5	85.0	1	82.5	3.0	3.0	8.5	2.0

[a] The molar methanol/oxygen ratio was 1:1.

Table 3

IR bands and assignments of the surface species formed in the methanol oxidation on the V_2O_5/TiO_2 catalyst.

Frequency, cm^{-1}	**Type of surface species**	**Type of vibration**	**Ref.**
1150	methoxy species	rocking $\rho(CH_3)$ mode	[9]
1360	bidentate formate species	symmetric stretching ν_s(O-C-O) mode	[9,13,53]
1433	methoxy species	symmetric deformation $\delta(CH_3)$ mode	[9]
1447	methoxy species	asymmetric deformation $\delta(CH_3)$ mode	[9]
1550	bidentate formate species	asymmetric stretching ν_{as}(O-C-O) mode	[9,13,53]
1655	methyl formate	stretching ν(C=O) mode	[9,13,53]
2825	methoxy species	Fermi resonance of $2\delta_s(CH_3)$	[9,13,47-53]
2847	molecular methanol	Fermi resonance of $2\delta_s(CH_3)$	[9]
2884	dioximethylene species	symmetric stretching $\nu_s(CH_2)$ mode	[50]
2923	dioximethylene species	asymmetric stretching $\nu_{as}(CH_2)$ mode	[50]
2931	methoxy species	symmetric stretching $\nu_s(CH_3)$ mode	[9,13,47-53]
2955	molecular methanol	symmetric stretching $\nu_s(CH_3)$ mode	[9]
2970	methoxy species	asymmetric stretching $\nu_{as}(CH_3)$ mode	[9]

Table 4

Binding energies and FWHMs of the Ti $2p_{3/2}$ and V $2p_{3/2}$ peaks shown in Figs. 7a, 8a, and 9; the relative intensity of different components (%) shown in parentheses.

Mixture	T, °C	FWHM of Ti $2p_{3/2}$, eV	V $2p_{3/2}$, eV (%)		
			V^{5+}	V^{4+}	V^{3+}
O_2	300	1.12	517.66 (100)	-	-
CH_3OH+O_2	100	1.05	517.73 (51)	516.50 (49)	-
CH_3OH+O_2	150	1.07	517.68 (59)	516.43 (41)	-
CH_3OH+O_2	200	1.09	517.63 (67)	516.40 (33)	-
CH_3OH	50	1.10	-	516.60 (41)	515.54 (59)
CH_3OH	100	1.12	-	516.60 (31)	515.42 (69)
CH_3OH	150	1.13	-	516.60 (28)	515.45 (72)
CH_3OH	200	1.14	-	516.50 (32)	515.47 (68)